

pubs.acs.org/NanoLett Letter

# Additive Opto-Thermomechanical Nanoprinting and Nanorepairing under Ambient Conditions

Md Shah Alam, Qiwen Zhan, and Chenglong Zhao\*



Cite This: https://dx.doi.org/10.1021/acs.nanolett.0c01261



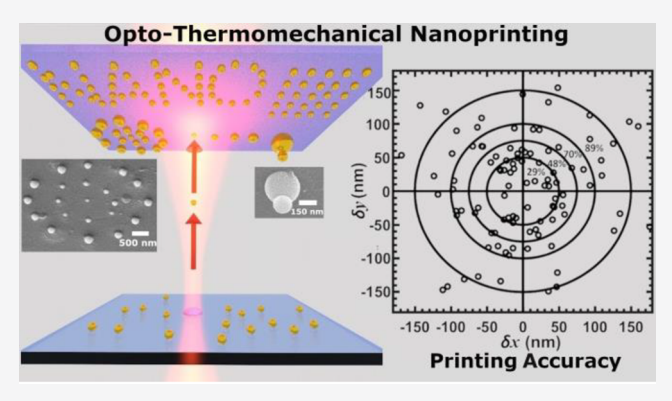
**ACCESS** I

Metrics & More

Article Recommendations

Supporting Information

ABSTRACT: We demonstrate an opto-thermomechanical (OTM) nanoprinting method that allows us not only to additively print nanostructures with sub-100 nm accuracy but also to correct printing errors for nanorepairing under ambient conditions. Different from other existing nanoprinting methods, this method works when a nanoparticle on the surface of a soft substrate is illuminated by a continuous-wave (cw) laser beam in a gaseous environment. The laser heats the nanoparticle and induces a rapid thermal expansion of the soft substrate. This thermal expansion can either release a nanoparticle from the soft surface for nanorepairing or transfer it additively to another surface in the presence of optical forces for nanoprinting with sub-100 nm accuracy. Details of the printing mechanism and parameters that affect the printing accuracy are investigated. This additive OTM nanoprinting



technique paves the way for rapid and affordable additive manufacturing or 3D printing at the nanoscale under ambient conditions.

KEYWORDS: additive manufacturing, nanoprinting, nanorepairing, laser printing, optothermal expansion, optical force

hree-dimensional printing or additive manufacturing, 1,2 which forms structures by adding materials layer upon layer, has attracted increasing attention due to its wide range of applications in various fields such as energy,<sup>3</sup> batteries,<sup>4</sup> structural electronics, 5,6 optoelectronics, 7,8 metamaterial, robotics, 10 microfluidics, 11 healthcare, 12 and drug delivery. 13 Lasers have been widely used in 3D printing for rapid prototyping at the macro- and microscales due to their excellent directivity for efficient energy delivery to the targeted materials. For example, microsized metallic particles can be selectively melted or sintered by a high-power laser beam to form complex 3D metal parts. However, it is challenging to directly downsize the existing macro- and microscale 3D printing techniques for nanoscale printing or nanoprinting.<sup>2</sup> Nanoparticles are ideal for serving as the raw materials for nanoprinting either in a liquid or a gaseous environment 17-19 due to their custom-designed large-volume and low-cost production with unique physical and chemical properties. 20,21 Nanoparticles can be attached to each other through electrostatic or van der Waals forces once they are in contact with each other. Therefore, 3D nanoprinting at the nanoscales can be realized by precisely manipulating and assembling individual nanoparticles to form the final structures.

Template-assisted methods, such as selective surface patterning<sup>22</sup> and capillary assembly,<sup>23</sup> have been used for 2D patterning of nanoparticles but requires multiple steps. Optical printing based on optical forces has been able to immobilize individual colloidal nanoparticles onto a substrate, but with

printing accuracy fundamentally limited by the Brownian motion of nanoparticles in a liquid environment and also limited to 2D manufacturing due to thermophoretic force.  $^{24-29}$  Laser-induced forward/backward transfer (LIFT/LIBT) techniques can be used to print 2D and 3D structures in a gaseous environment, but pulsed lasers have to be used.  $^{30-33}$  The electrohydrodynamic printing technique has the ability to print 3D nanostructures using nanoparticle solution as ink but lacks the capability of individual nanoparticle control and requires a conductive surface to work with.  $^{34}$ 

Here, we demonstrate an additive opto-thermomechanical nanoprinting (OTM-NP) technique that has the potential to overcome the aforementioned limitations for 3D printing on a nanoscale. The working mechanism and the parameters that affect the printing accuracy are discussed in detail. The OTM-NP has the following unique features: (1) both dielectric and metallic nanoparticles can be printed onto any type of substrate; (2) printing errors can be corrected; (3) cw laser is used instead of a pulsed laser; and (4) both nanoprinting

Received: March 22, 2020 Revised: June 4, 2020 Published: June 5, 2020



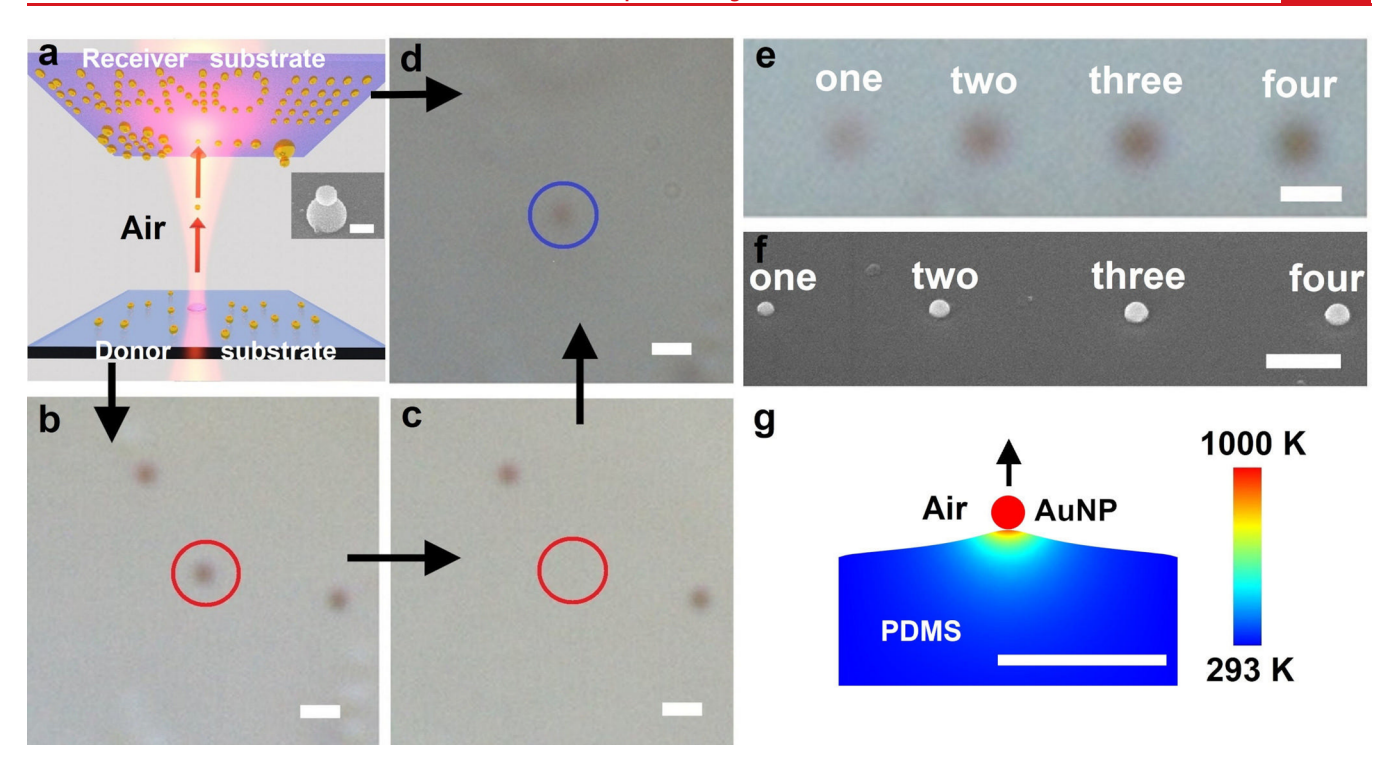


Figure 1. Mechanism of opto-thermomechanical nanoprinting (OTM-NP) and demonstration of additive nanoprinting. (a) Schematic of OTM-NP. The inset scale bar represents 150 nm. (b) Three 100 nm AuNPs on a PDMS donor substrate. The AuNP in the red circle will be released from the donor substrate. (c) The AuNP in the red circle is released from the surface after the laser is turned on (disappeared from the red circle). (d) The released AuNP is transferred to a receiver substrate, as shown in the blue circle. (e, f) optical and SEM images of additive printing of one, two, three, and four individual 100 nm AuNPs (from left to right) at the same position on a receiver substrate, respectively. (g) FEM simulation of temperature distribution and thermal expansion of the PDMS substrate for a 100 nm AuNP under laser illumination. Scale bars represent 500 nm.

and nanorepairing are conducted in the air that can avoid potential contaminations in a liquid environment.

Figure 1a schematically shows the OTM-NP process. The gold nanoparticle solution is first diluted, then drop-casted, and naturally dried on a donor substrate that consists of a soft, thin layer of polydimethylsiloxane (PDMS) on a glass coverslip. Figure S1 shows dispersed gold nanoparticles (AuNPs) on the donor substrates. A cw laser operating at a 1064 nm wavelength and an oil-immersion objective to focus the laser beam were used in this OTM-NP. The details of the optical setup (Figure S2) are described in the Materials and Methods section. A targeted 100 nm AuNP, as shown in the red circle of Figure 1b, is brought to the laser focus by using a nanopositioning stage, while the laser beam is OFF. The AuNP is released from the donor substrate when the laser is turned ON (Figure 1c). The released nanoparticle is eventually transferred and printed onto a receiver substrate placed very close to the donor substrate (Figure 1d). Movies S1 and S2 show the details of this transfer process.

Individual AuNPs can be released in sequence and transferred additively onto a receiver substrate. Figure 1e,f shows the optical and SEM images of additive printing of one, two, three, and four individual 100 nm AuNPs (from left to right) at the same position on a glass substrate. The AuNPs are printed on top of the prior-printed AuNPs and merged together to form a larger particle depending on the number of AuNPs printed. The volumes of the resultant particles are directly proportional to the number of particles printed on the same positions of the receiver substrate. The laser intensity of  $100 \text{ mW}/\mu\text{m}^2$  was used to release and print the 100 nm AuNPs in this experiment. It should be noted that it is possible

to control the laser intensity so that the later-printed AuNPs are printed on top of the prior-printed one rather than merged together. The inset in Figure 1a shows such a structure by additively printing ten individual 150 nm AuNPs. The first nine AuNPs merge to form a base particle, and the tenth AuNP lands on top of it.

The OTM-NP involves basic light-matter interaction along with thermomechanical behaviors of the substrate, particlesurface interaction, and particle dynamics. Polymer materials (PDMS in our experiments) are highly flexible and elastic, and have comparatively large linear thermal expansion coefficients  $(3.2 \times 10^{-4} \, {}^{\circ}\text{C}^{-1})$  for PDMS), which can provide significant thermal expansion force near their surface when exposed to a sudden temperature change due to the laser heating of the AuNPs, as shown in the finite element method (FEM) simulation (Figure 1g). The mechanism of OTM-NP is schematically shown in Figure 2. A metallic nanoparticle (AuNP in our experiment) attaches to the surface of the donor substrate (PDMS in our experiments) by van der Waals attractive force  $(F_{\nu})$  after it is dried in the air (Figure 2a). The gravitational force on the AuNP is negligible as it is around 6 orders of magnitude smaller than the van der Waals force. When the AuNP is illuminated by a focused laser beam, it absorbs the laser energy and heats the donor substrate beneath it, which causes rapid thermal expansion of the donor substrate. The thermal expansion rate of the substrate depends on the thermal expansion coefficient of the substrate material and the applied laser intensity. The rapid thermal expansion of the PDMS surface applies a thermal expansion force  $(F_{\rm TE})$ (Figure 2b). The AuNP also experiences an optical axial force  $(F_z)$  and an optical gradient force  $(F_G)^{35-37}$  due to the focused

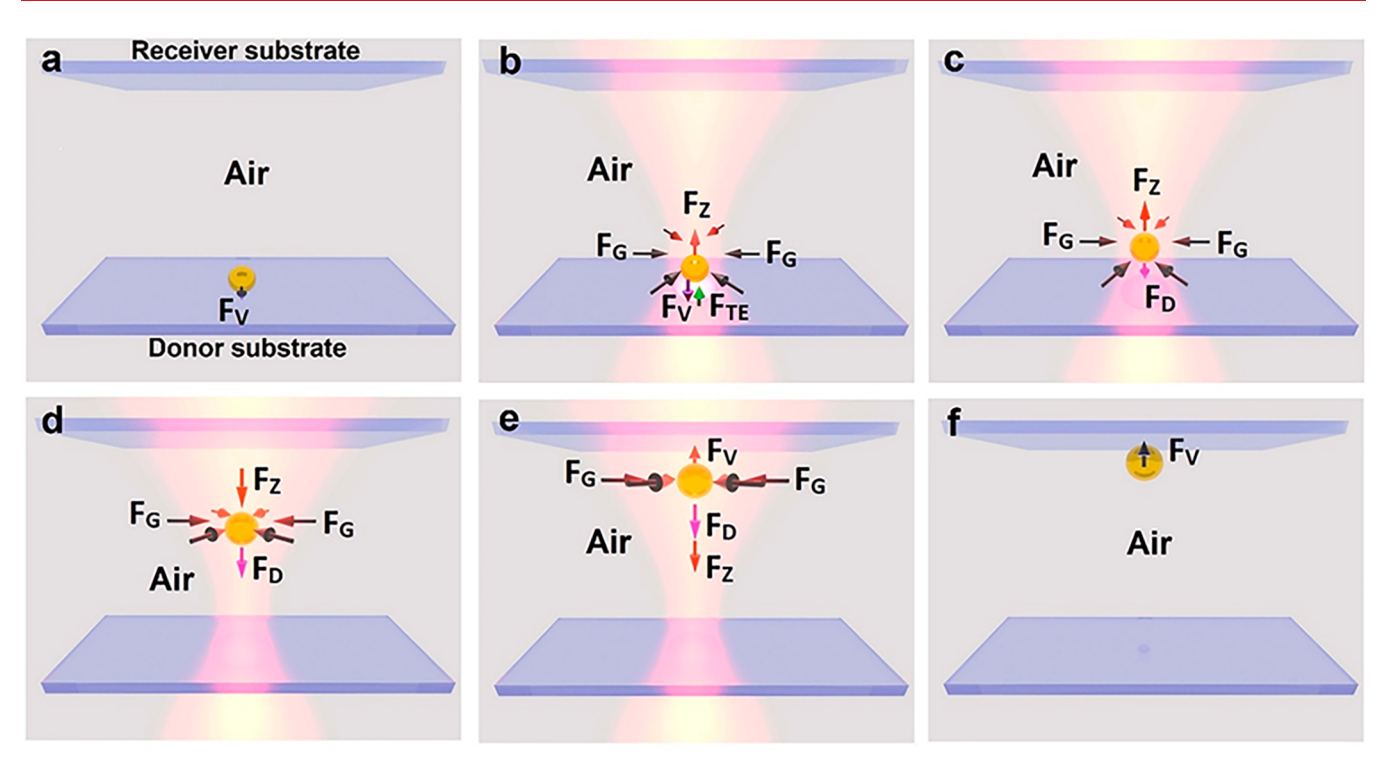


Figure 2. Schematic of the OTM-NP process. The arrows indicate the directions of different types of forces acting on the AuNP. (a) AuNP attaches to the surface of the donor substrate due to the van der Waals attraction force  $(F_v)$ . (b) Thermal expansion force  $(F_{TE})$  is applied to the AuNP due to the thermal expansion of the soft substrate after the laser is turned on. The focused laser beam also exerts an optical axial force  $(F_z)$  and optical gradient force  $(F_G)$  to the AuNP. (c) The AuNP acquires enough momentum, overcomes the van der Waals force, and starts to move toward the very closely placed  $(\sim 1 \, \mu \text{m gap})$  receiver substrate in the presence of optical axial force  $(F_z)$  and optical gradient force  $(F_G)$ . The drag force  $(F_D)$  opposes the motion of the AuNP. (d) The direction of the optical axial force flips when the AuNP is a few hundred nanometers away from the center of the focus. (e) The receiver substrate attracts the AuNP when it reaches close to the receiver substrate. (f) The AuNP reaches the receiver substrate and printed on it due to van der Waals attraction force.

laser beam. Here, the optical axial force  $F_z$  is the total force including the optical scattering force and gradient force in the laser propagating direction. However, the optical forces are negligible at the beginning of the process as the van der Waals force is around 2 orders of magnitude larger than the optical forces. In the early stage of the surface deformation, the nanoparticle moves together with the expanding substrate (Figure 2b). Before reaching a steady state temperature, the velocity of the nanoparticle continues rising with the increasing expansion rate of the substrate (Figure S3a,b). Eventually, the thermal expansion rate of the substrate, as well as the velocity of the AuNP, reaches their peaks (Figure S3b). Then, the thermal expansion rate of the substrate starts to decrease, which reduces the velocity of the AuNP due to the van der Waals attraction force. However, the AuNP tends to move upward at a constant velocity due to inertia. As a result, an inertial force is applied to the AuNP. At a certain point, the thermal expansion rate of the substrate is low enough compared to the gained momentum of the AuNP such that the inertial force exceeds the van der Waals attraction force. Therefore, the AuNP is released from the donor substrate and moves upward (Figure S3b, Figure 2c) in the presence of

The AuNP continues moving toward the very closely placed receiver substrate due to the inertia and the optical axial force  $(F_z)$ , as illustrated in Figure 2c. The transverse optical gradient force  $(F_G)$  helps to push the AuNP toward the optical axis and improves the printing accuracy. The laser is focused a few hundreds of nanometers above the AuNP. Therefore, the

optical axial force  $(F_z)$  on the AuNP is first upward, assisting in the AuNP release process and then changes its direction to downward (Figure 2c,d). The air drag force  $(F_D)$  on the AuNP always opposes the AuNP motion and slows down the AuNP. However, the AuNP keeps moving toward the receiver substrate due to the inertia. The temperature of the AuNP and the substrate drop after the AuNP is released from the substrate because the AuNP moves away from the laser focus as shown in Figure S3a, which causes the shrinking of the substrate, and the substrate finally returns to its normal state due to its high elasticity. As the AuNP approaches the receiver substrate, the van der Waals force between the AuNP and the receiver substrate becomes significant. Therefore, the AuNP is attracted toward the receiver substrate (Figure 2e) and finally printed onto it (Figure 2f).

The AuNP can desorb from a flexible donor substrate but cannot desorb from a hard substrate, such as a glass substrate (Figure S4), due to the relatively small linear thermal expansion coefficient of the glass,  $7.6 \times 10^{-6}$  C<sup>1-.38</sup> Therefore, the material of the donor substrate plays an important role in the OTM-NP, and the proper choice of the donor substrate depends on the optical property of the nanoparticles to be printed. The following guidelines can be used for the choice of the donor substrate: (1) If the nanoparticles to be printed are absorptive to the laser (such as AuNPs), a transparent and flexible substrate (such as the PDMS) can be used as the donor substrate, or (2) if the nanoparticles are transparent to the laser (such as dielectric nanoparticles), an absorptive substrate can be used as the donor substrate. Figure S5 shows the printing of

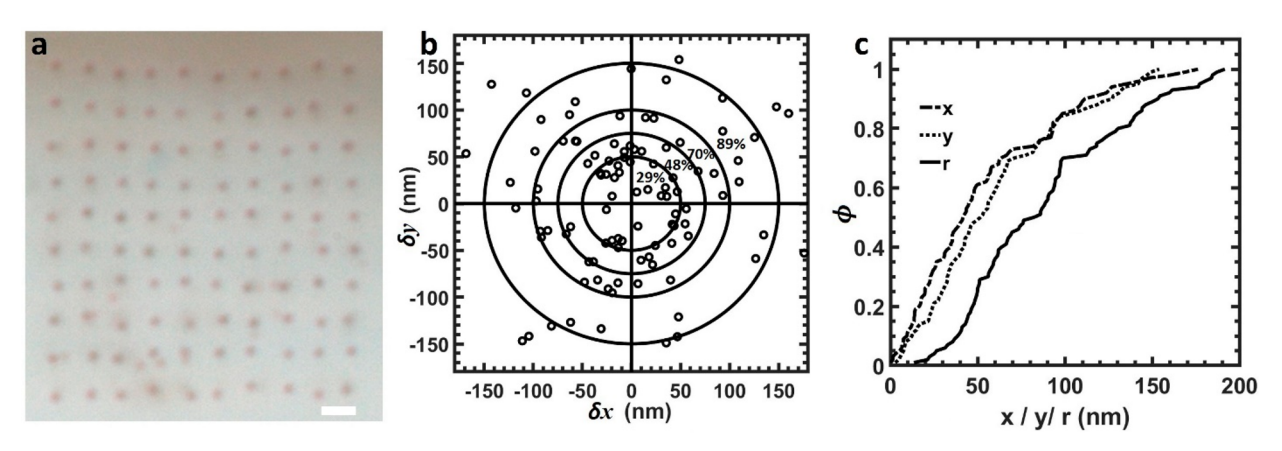
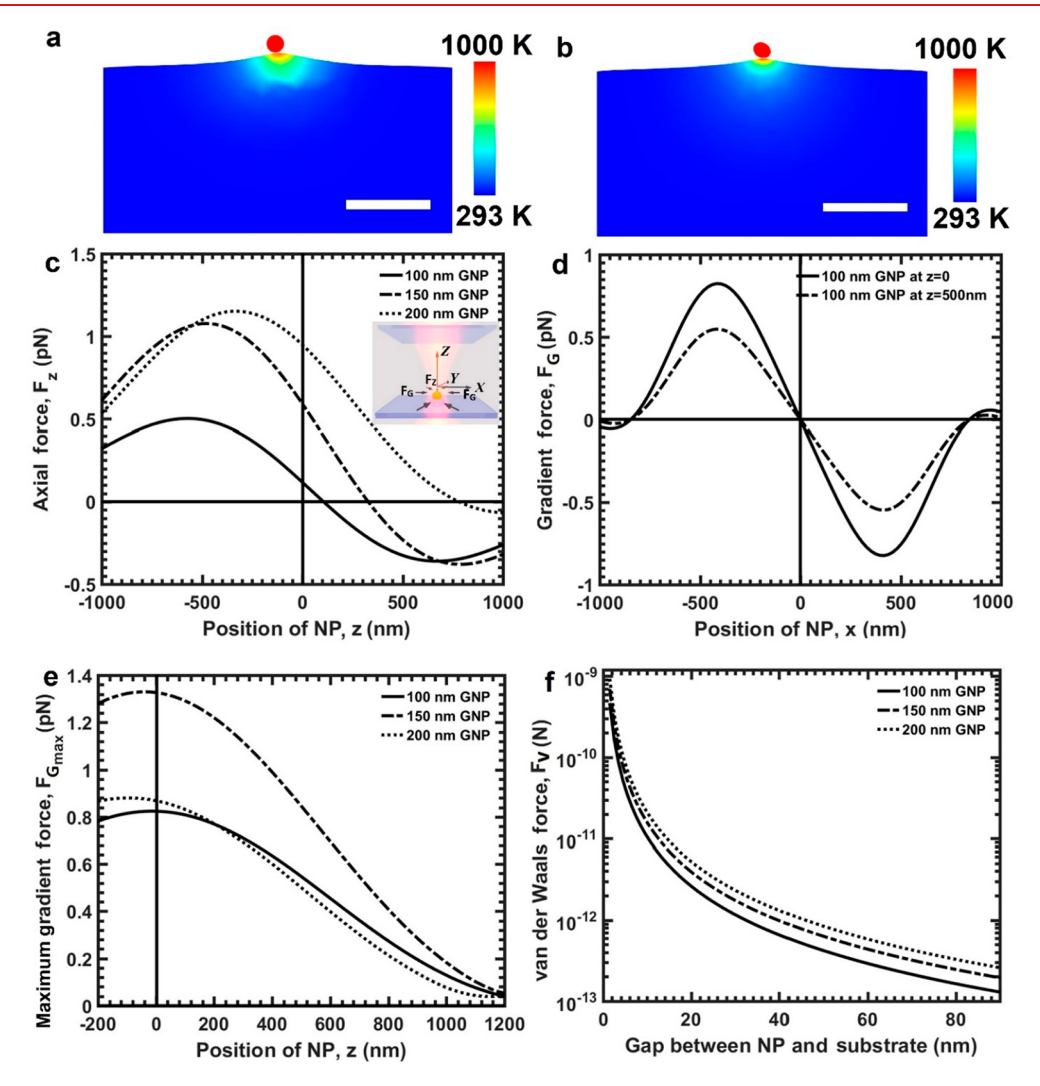


Figure 3. Printing accuracy of OTM-NP. (a) A 10  $\times$  10 array of 100 nm AuNPs printed on a glass substrate. Scale bar represents 1  $\mu$ m. (b) Scatter plot of the printing error in the x-y plane. (c) x, y, and radial (r) cumulative distribution function of the printing error.



**Figure 4.** (a, b) FEM simulation of the temperature distribution and thermal expansion of a PDMS substrate. (a) Effect of inhomogeneity of the donor substrate. (b) Effect of the particle shape. Scale bars represent 500 nm. (c–e) Optical force on a AuNP. Optical forces are calculated at a laser power of 55, 26, and 7 mW as that applied on 100, 150, and 200 nm AuNPs in the experiment, respectively. Here, the origin of the coordinate (x = 0, y = 0, x = 0) is the center of laser focus, and the z-axis (x = 0, y = 0) is the optical axis. (c) Optical axial force on 100, 150, and 200 nm AuNPs. The axial force is positive, at its maximum, below the center of focus. The inset shows the schematic of optical forces. (d) Optical gradient force on a 100 nm AuNP at the focal plane (xy-plane at z = 0) and 500 nm away from the focal plane (xy-plane at x = 0) The maximum value of the gradient force on 100, 150 and 200 nm AuNPs at different xy-planes (xy). (f) The van der Waals attractive force on 100, 150, and 200 nm AuNPs.

dielectric silica  $(SiO_2)$  nanoparticles from an indium tin oxide (ITO)-coated polyethylene terephthalate (PET) donor substrate. Here, ITO absorbs the laser energy and causes thermal expansion of PET.

A similar technique, blister-based laser-induced forward transfer (BB-LIFT), has been demonstrated to release particles or liquid ink from an absorbing/metal film by using pulsed lasers as a result of thermal expansion/deformation of the substrate.<sup>39–41</sup> However, the OTM-NP has the following different features compared to the BB-LIFT: (1) A fs or ns pulsed laser is used in the BB-LIFT method, while a continueswave (cw) laser is used in the OTM-NP. (2) An absorptive/ metal film is used in the BB-LIFT, while a transparent soft substrate (PDMS on glass) is used in the OTM-NP of absorptive nanoparticles. (3) The required laser intensity to release nanoparticles with OTM-NP is lower than that with BB-LIFT.<sup>39</sup> (4) As the substrate is transparent and the metal nanoparticle is responsible for generating heat by laser absorption, the size of the heat affected zone (HAZ) in OTM-NP is smaller than that in BB-LIFT; and (5) the center of thermal expansion in BB-LIFT is located at the center of the incident laser beam on the substrate, while the peak position of the thermal expansion of the substrate in OTM-NP is located at the contact point of the absorptive nanoparticle and the substrate, which helps to release the nanoparticle normal to the donor substrate (Figure 1g). Therefore, the OTM-NP technique can print a single nanoparticle with nanoscale accuracy.

A 10 × 10 array of 100 nm AuNPs is printed on a glass substrate by using the OTM-NP, as shown in Figure 3a. A laser intensity of 100 mW/ $\mu$ m<sup>2</sup> and a gap of ~1  $\mu$ m between the donor and the receiver substrates are used in the experiment. Figure 3b shows the scatter plot of the printing error in the xand y dimensions (transverse to the laser propagation direction). The printing error of each particle is evaluated by calculating the deviation of the center of mass of the image of the *i*<sup>th</sup> printed particle  $(x_i, y_i)$  from a targeted position  $(x_{i0}, y_{i0})$ . Therefore, the printing errors along x, y, and the radial rdirection for the ith nanoparticle are  $(\partial x_i, \partial y_i, \partial r_i) = (x_i - x_{i0}, y_i - y_{i0}, \sqrt{\partial x_i^2 + \partial y_i^2}),$  respectively. The concentric circles in Figure 3b represent that 29%, 48%, 70%, and 89% particles are printed within printing errors of 50, 75, 100, and 150 nm, respectively. According to Figure 3b, 70% of the particles are printed with sub-100 nm accuracy. An alternative way of illustrating the printing accuracy and error is the cumulative probability distribution function  $\varphi$  of the printing, which represents the probability that a nanoparticle will be printed within a certain range from the target position. Figure 3c shows the 1D cumulative probability distribution functions  $\varphi(x)$ ,  $\varphi(y)$ , and  $\varphi(r)$ . The standard deviations of the printing error in the x, y, and radial r directions are  $S_r = 68$  nm,  $S_v = 71$  nm, and  $S_r = 99$  nm, respectively. This printing accuracy is related to this specific experiment only and is comparable to the printing accuracy of LIFT/LIBT methods. 30-33,42 Higher printing accuracy has been achieved in the additive printing of one, two, three, four, and ten individual AuNPs at the same positions on a receiver substrate as shown in Figure 1f and inset of Figure 1a, respectively. The printing accuracy of the OTM-NP method is affected by the parameters such as the homogeneity of donor substrate, nanoparticle shape, laser polarization, optical force, and the gap between the donor and receiver substrates. In comparison, the printing accuracy of the LIFT/LIBT is affected by parameters such as film thickness, laser focal spot size, laser pulse energy, and laser wavelength. In addition, the size of the printed nanoparticles with LIFT/LIBT is comparatively larger than that with OTM-NP, because the HAZ in LIFT/LIBT depends on the size of the diffraction-limited laser focal spot. In contrast, the HAZ in OTM-NP depends on the size of the AuNP, which can be smaller than that in LIFT/LIBT.

The homogeneity of the donor substrate is very important for symmetric heat conduction and thermal expansion around the nanoparticle. 43-46 Symmetric thermal expansion around a spherical nanoparticle provides the nanoparticle with a momentum normal to the donor substrate's surface; therefore, it helps to transfer the nanoparticle vertically toward the target position on the receiver substrate. In contrast, an asymmetric thermal expansion causes the nanoparticle to release with an angle to the surface normal, resulting in a printing error. Figure S6 and Movie S3 show the asymmetric thermal expansion of the donor substrate around the AuNP due to the inhomogeneity of the donor substrate. Figure 4a shows the simulated temperature distribution of an inhomogeneous PDMS substrate as a result of heating a 100 nm spherical AuNP. The position of the maximum expansion of the substrate surface, where the thermal expansion force is exerted on the nanoparticle, is not aligned with the center-of-mass of the AuNP (Figure 4a). Therefore, the AuNP will be released at an angle to the normal of the donor substrate's surface. In contrast, the heating of a homogeneous substrate will allow the release of the AuNP normal to the surface (Figure 1g). In our experiment, the PDMS solution was prepared by adding the curing agent to the elastomer base of Dow SYLGARD 184 in a 1:10 (w/w) ratio. To achieve homogeneous PDMS film, the solution was mixed thoroughly by a magnetic stirrer inside an airtight flask for around 10 h and sonicated for 30 min. A ~10  $\mu$ m thick homogeneous PDMS layer was then spin-coated on a glass coverslip at a spin speed of 7000 rpm for 1 min.<sup>47</sup>

While we have shown the successful printing of 100 nm ultrauniform spherical AuNPs with sub-100 nm accuracy, it is challenging to print 200 nm imperfect spherical AuNPs (Figure S7a) with such accuracy. The imperfect spherical shape of a 200 nm AuNP causes asymmetric temperature distribution in a donor substrate and misalignment between the maximum thermal expansion position and the center-ofmass of the AuNP. Figure 4b shows the simulation of the temperature distribution and thermal expansion of a PDMS substrate as a result of the heating of an elliptical AuNP. Moreover, the air drag force on an imperfect spherical nanoparticle also affects the trajectory of the nanoparticle in the transfer process. However, the printing accuracy of imperfect spherical 200 nm AuNPs can be significantly improved by preheating. In the preheating technique, a 200 nm AuNP is first preheated with a laser intensity of 4 mW/  $\mu$ m<sup>2</sup>, and then the intensity is quickly increased to 11 mW/  $\mu m^2$  to desorb the AuNP from the donor substrate. One possible reason for the improvement of printing accuracy with preheating is that the preheating helps to round the edges of the imperfect spherical AuNP<sup>48,49</sup> and makes it comparatively more spherical. Movie S4 shows that AuNP shrinks after preheating and looks more spherical. A 5 × 3 array of 200 nm AuNPs is printed by using the preheating technique (Figure

The use of a circularly polarized laser beam can further improve the printing accuracy. In our experiment, a quarter-

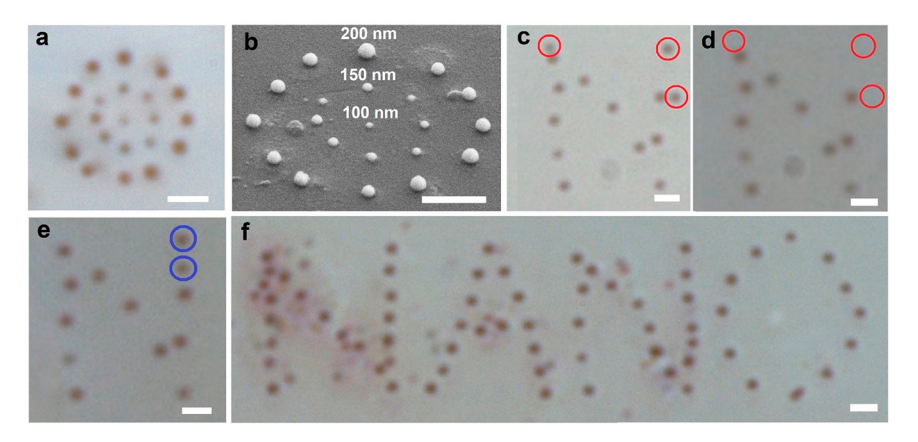


Figure 5. Additive nanoprinting and nanorepairing. (a) Optical image of a circular pattern that is formed by selectively printing of three different sizes of AuNPs (100, 150, and 200 nm) on a glass substrate. (b) SEM image of the corresponding structure. (c) A letter "N" consisting of 200 nm AuNPs is printed on an ITO-coated glass substrate using preheating. The gap between the donor and the receiver substrate was  $\sim 1.5 \ \mu m$ . The AuNPs inside the three red circles are selected to be removed. (d) Three AuNPs are removed from the substrate. (e) Two AuNPs (in the blue circles) are added to the letter "N". (f) Optical image of the word "NANO" consisting of 200 nm AuNPs that is formed by applying OTM nanoprinting and nanorepairing process. Scale bars represent 1  $\mu m$ .

wave plate is used to convert the laser polarization from linear to circular, which provides a symmetric focal spot because of the reduced depolarization of the oil-immersion objective <sup>50,51</sup> (Figure S8). The focal spot of a linearly polarized laser beam from an oil-immersion objective lens is elongated in the direction of the laser polarization. The symmetric focal spot helps in symmetric temperature distribution around the nanoparticle that results in higher printing accuracy.

Illuminating a AuNP with a focused laser beam not only increases the temperature of the AuNP but also exerts an optical force on the AuNP, which can improve the printing accuracy. Figure 4c,d represents the calculated optical axial forces  $(F_z)$  and transverse optical gradient force  $(F_G)$  on a 100, 150, and 200 nm AuNP, respectively. The optical forces  $(F_{zz})$  $F_{\rm G}$ ) exerted on a AuNP with a size ranging from 100 to 200 nm is on the order of pico-Newtons (pN) depending on the laser power. The van der Waals force between a PDMS substrate and a AuNP with a size ranging from 100 to 200 nm is on the order of nano-Newton (nN) depending on the gap between the nanoparticle and substrate's surface (Figure 4f). Therefore, a AuNP cannot be released from a PDMS donor substrate by only the optical force. The van der Waals attractive force dominates until the AuNP leaves the substrate. Once the AuNP leaves the donor substrate due to the thermal expansion force, the optical force can be used to improve the printing accuracy. Figure 4e shows the maximum transverse optical gradient force ( $F_{G_{max}}$ ) for a 100, 150, and 200 nm AuNP as the AuNP moves toward the receiver substrate in the zdirection. The AuNP experiences higher  $F_{G_{\max}}$  around the focal plane (z = 0 in Figure 4e). Therefore, focusing the laser beam a few hundred nanometers above the AuNP helps to decrease the spreading angle of the AuNP as it moves toward the receiver substrate. Sub-100 nm printing accuracy has been achieved by focusing a laser beam slightly above the AuNP.

The gap between the donor and receiver substrates also has a direct effect on the printing accuracy. A smaller gap reduces the printing error because the amount of deviation of the landed particle from its targeted position on the receiver substrate is directly proportional to the gap distance between the donor and receiver substrates. The gap was kept at  $\sim\!1~\mu{\rm m}$  in our experiments unless stated otherwise.

The wide variety of commercially available nanoparticles provides an affordable and unlimited supply of raw materials for the OTM-NP. Nanoprinting can be realized by either additively printing the same size (Figure 1e,f) or selectively printing different sizes of nanoparticles (Figure 5a,b). Figure 5a,b represents the optical and SEM image of a circular structure that is printed on a glass substrate by printing one 100 nm AuNP at the center, eight 150 nm AuNPs in the first ring, and twelve 200 nm AuNPs in the second ring. The laser intensities used for the printing of 100, 150, and 200 nm AuNPs are 100 mW/ $\mu$ m<sup>2</sup>, 40 mW/ $\mu$ m<sup>2</sup>, and 11 mW/ $\mu$ m<sup>2</sup>, respectively.

The desorption process of the OTM-NP can also be used to correct printing errors for nanorepairing as shown in Figure 5c—e. The letter "N" is first printed by additive printing of fourteen 200 nm AuNPs on an ITO-coated glass substrate with preheating (Figure 5c). To repair the pattern "N", three AuNPs (marked in the red circles) are selectively removed from the letter (Figure 5d). Then two new AuNPs (marked in the blue circles) are added to the letter "N" to repair the structure as shown in Figure 5e. Both the nanoprinting and the nanorepairing can be conducted on the same platform under ambient conditions. Figure 5f shows the optical image of the word "NANO" consisting of 200 nm AuNPs that are printed and corrected by using the OTM-NP and the nanorepairing technique.

In conclusion, an affordable OTM-NP method that allows for both additive nanoprinting and nanorepairing with sub-100 nm accuracy has been successfully demonstrated. The working mechanism and guidelines for improving the printing accuracy are discussed in detail. This method has the following unique features: First, the OTM-NP is accomplished in the air with a cw laser, which allows for rapid and affordable prototyping of nanoscale structures without contaminating the receiver substrate. In contrast, optical printing based on optical forces requires a liquid environment. Laser-induced forward/backward transfer (LIFT/LIBT) methods are realized in gaseous environments, but expensive pulsed lasers are required. Second, the OTM-NP can print nanoparticles of different types and sizes in sequence either to form 2D structures or merge the nanoparticles to form structures in a direction that is normal to the printing substrate. Therefore,

this technique can be potentially used for the fabrication of 2D and 3D electronic and optical devices such as metasurface or even 3D metamaterial. Finally, it can be potentially used as a nanorepairing tool to correct printing errors that are inevitable and challenging to correct.

## ASSOCIATED CONTENT

# Supporting Information

The Supporting Information is available free of charge at https://pubs.acs.org/doi/10.1021/acs.nanolett.0c01261.

Dispersed gold nanoparticles (AuNPs) on a donor substrate; experimental setup for the OTM-NP; FEM simulation of the temperature, thermal expansion rate, and velocity of AuNP and PDMS substrate; nanoparticle cannot be released from a glass substrate; printing dielectric- silica (SiO $_2$ ) nanoparticle from absorptive donor substrate; asymmetric thermal expansion of the donor substrate around the AuNP due to inhomogeneity of donor substrate; effect of preheating on imperfect spherical AuNP; the focal spots of a linearly polarized and circularly polarized laser beam (PDF)

Movie S1 (AVI)

Movie S2 (AVI)

Movie S3 (AVI)

Movie S4 (AVI)

## AUTHOR INFORMATION

#### **Corresponding Author**

Chenglong Zhao — Department of Electro-Optics and Photonics and Department of Physics, University of Dayton, Dayton, Ohio 45469, United States; orcid.org/0000-0003-2831-1671; Email: czhao1@udayton.edu

### **Authors**

Md Shah Alam — Department of Electro-Optics and Photonics, University of Dayton, Dayton, Ohio 45469, United States; orcid.org/0000-0003-3694-0267

Qiwen Zhan — Department of Electro-Optics and Photonics, University of Dayton, Dayton, Ohio 45469, United States; orcid.org/0000-0001-8745-4213

Complete contact information is available at: https://pubs.acs.org/10.1021/acs.nanolett.0c01261

#### Notes

The authors declare no competing financial interest.

#### ACKNOWLEDGMENTS

The authors acknowledge the financial support from the National Science Foundation under award number CMMI-1761132 and the Graduate Student Summer Fellowship provided by the Graduate Academic Affairs of the University of Dayton.

# **■** REFERENCES

- (1) Lin, L.; Kollipara, P. S.; Zheng, Y. Digital Manufacturing of Advanced Materials: Challenges and Perspective. *Mater. Today* **2019**, 28, 49–62.
- (2) Hirt, L.; Reiser, A.; Spolenak, R.; Zambelli, T. Additive Manufacturing of Metal Structures at the Micrometer Scale. *Adv. Mater.* **2017**, 29, 1604211.
- (3) Fu, K.; Yao, Y.; Dai, J.; Hu, L. Progress in 3D Printing of Carbon Materials for Energy-Related Applications. *Adv. Mater.* **2017**, *29*, 1603486.

- (4) Sun, K.; Wei, T.-S.; Ahn, B. Y.; Seo, J. Y.; Dillon, S. J.; Lewis, J. A. 3D Printing of Interdigitated Li-Ion Microbattery Architectures. *Adv. Mater.* **2013**, *25*, 4539–4543.
- (5) Tan, H. W.; An, J.; Chua, C. K.; Tran, T. Metallic Nanoparticle Inks for 3D Printing of Electronics. *Adv. Electron. Mater.* **2019**, *5*, 1800831.
- (6) Macdonald, E.; Salas, R.; Espalin, D.; Perez, M.; Aguilera, E.; Muse, D.; Wicker, R. B. 3D Printing for the Rapid Prototyping of Structural Electronics. *IEEE Access* **2014**, *2*, 234–242.
- (7) Loke, G.; Yuan, R.; Rein, M.; Khudiyev, T.; Jain, Y.; Joannopoulos, J.; Fink, Y. Structured Multimaterial Filaments for 3D Printing of Optoelectronics. *Nat. Commun.* **2019**, *10*, 4010.
- (8) Kong, Y. L.; Tamargo, I. A.; Kim, H.; Johnson, B. N.; Gupta, M. K.; Koh, T.-W.; Chin, H.-A.; Steingart, D. A.; Rand, B. P.; McAlpine, M. C. 3D Printed Quantum Dot Light-Emitting Diodes. *Nano Lett.* **2014**, *14*, 7017–7023.
- (9) Kadic, M.; Milton, G. W.; van Hecke, M.; Wegener, M. 3D Metamaterials. *Nat. Rev. Phys.* **2019**, *1*, 198–210.
- (10) Wallin, T. J.; Pikul, J.; Shepherd, R. F. 3D Printing of Soft Robotic Systems. *Nat. Rev. Mater.* **2018**, *3*, 84–100.
- (11) Bhattacharjee, N.; Urrios, A.; Kang, S.; Folch, A. The Upcoming 3D-Printing Revolution in Microfluidics. *Lab Chip* **2016**, 16, 1720–1742.
- (12) Colaco, M.; Igel, D. A.; Atala, A. The Potential of 3D Printing in Urological Research and Patient Care. *Nat. Rev. Urol.* **2018**, *15*, 213–221.
- (13) Capel, A. J.; Rimington, R. P.; Lewis, M. P.; Christie, S. D. R. 3D Printing for Chemical, Pharmaceutical and Biological Applications. *Nat. Rev. Chem.* **2018**, *2*, 422–436.
- (14) King, W. E.; Anderson, A. T.; Ferencz, R. M.; Hodge, N. E.; Kamath, C.; Khairallah, S. A.; Rubenchik, A. M. Laser Powder Bed Fusion Additive Manufacturing of Metals; Physics, Computational, and Materials Challenges. *Appl. Phys. Rev.* **2015**, *2*, 041304.
- (15) Khairallah, S. A.; Anderson, A. T.; Rubenchik, A.; King, W. E. Laser Powder-Bed Fusion Additive Manufacturing: Physics of Complex Melt Flow and Formation Mechanisms of Pores, Spatter, and Denudation Zones. *Acta Mater.* **2016**, *108*, 36–45.
- (16) Ly, S.; Rubenchik, A. M.; Khairallah, S. A.; Guss, G.; Matthews, M. J. Metal Vapor Micro-Jet Controls Material Redistribution in Laser Powder Bed Fusion Additive Manufacturing. *Sci. Rep.* **2017**, *7*, 4085.
- (17) Zhao, C.; Shah, P. J.; Bissell, L. J. Laser Additive Nano-Manufacturing under Ambient Conditions. *Nanoscale* **2019**, *11*, 16187–16199.
- (18) Li, J.; Hill, E. H.; Lin, L.; Zheng, Y. Optical Nanoprinting of Colloidal Particles and Functional Structures. *ACS Nano* **2019**, *13* (4), 3783–3795.
- (19) Alam, M. S.; Zhao, C. Nondestructive Approach for Additive Nanomanufacturing of Metallic Nanostructures in the Air. ACS Omega 2018, 3 (1), 1213–1219.
- (20) Xia, Y.; Xiong, Y.; Lim, B.; Skrabalak, S. E. Shape-Controlled Synthesis of Metal Nanocrystals: Simple Chemistry Meets Complex Physics? *Angew. Chem., Int. Ed.* **2009**, *48* (1), 60–103.
- (21) Sun, Y.; Science, Y. X. Shape-Controlled Synthesis of Gold and Silver Nanoparticles. *Science* **2002**, *298*, 2176–2179.
- (22) Fan, F.; Stebe, K. J. Assembly of Colloidal Particles by Evaporation on Surfaces with Patterned Hydrophobicity. *Langmuir* **2004**, *20* (8), 3062–3067.
- (23) Flauraud, V.; Mastrangeli, M.; Bernasconi, G. D.; Butet, J.; Alexander, D. T. L.; Shahrabi, E.; Martin, O. J. F.; Brugger, J. Nanoscale Topographical Control of Capillary Assembly of Nanoparticles. *Nat. Nanotechnol.* **2017**, *12* (1), 73–80.
- (24) Guffey, M. J.; Scherer, N. F. All-Optical Patterning of Au Nanoparticles on Surfaces Using Optical Traps. *Nano Lett.* **2010**, *10* (11), 4302–4308.
- (25) Nedev, S.; Urban, A. S.; Lutich, A. A.; Feldmann, J. Optical Force Stamping Lithography. *Nano Lett.* **2011**, *11*, 5066–5070.
- (26) Gargiulo, J.; Violi, I. L.; Cerrota, S.; Chvátal, L.; Cortés, E.; Perassi, E. M.; Diaz, F.; Zemánek, P.; Stefani, F. D. Accuracy and

- Mechanistic Details of Optical Printing of Single Au and Ag Nanoparticles. ACS Nano 2017, 11, 9678–9688.
- (27) Gargiulo, J.; Cerrota, S.; Cortés, E.; Violi, I. L.; Stefani, F. D. Connecting Metallic Nanoparticles by Optical Printing. *Nano Lett.* **2016**, *16*, 1224–1229.
- (28) Do, J.; Fedoruk, M.; Jäckel, F.; Feldmann, J. Two-Color Laser Printing of Individual Gold Nanorods. *Nano Lett.* **2013**, *13*, 4164–4168.
- (29) Urban, A. S.; Lutich, A. A.; Stefani, F. D.; Feldmann, J. Laser Printing Single Gold Nanoparticles. *Nano Lett.* **2010**, *10*, 4794–4798.
- (30) Zhigunov, D. M.; Evlyukhin, A. B.; Shalin, A. S.; Zywietz, U.; Chichkov, B. N. Femtosecond Laser Printing of Single Ge and SiGe Nanoparticles with Electric and Magnetic Optical Resonances. *ACS Photonics* **2018**, *5*, 977–983.
- (31) Serra, P.; Piqué, A. Laser-Induced Forward Transfer: Fundamentals and Applications. *Adv. Mater. Technol.* **2019**, *4*, 1800099.
- (32) Zywietz, U.; Evlyukhin, A. B.; Reinhardt, C.; Chichkov, B. N. Laser Printing of Silicon Nanoparticles with Resonant Optical Electric and Magnetic Responses. *Nat. Commun.* **2014**, *5*, 3402.
- (33) Kuznetsov, A. I.; Kiyan, R.; Chichkov, B. N. Laser Fabrication of 2D and 3D Metal Nanoparticle Structures and Arrays. *Opt. Express* **2010**, *18* (20), 21198.
- (34) Galliker, P.; Schneider, J.; Eghlidi, H.; Kress, S.; Sandoghdar, V.; Poulikakos, D. Direct Printing of Nanostructures by Electrostatic Autofocussing of Ink Nanodroplets. *Nat. Commun.* **2012**, *3*, 890.
- (35) Ashkin, A. Acceleration and Trapping of Particles by Radiation Pressure. *Phys. Rev. Lett.* **1970**, 24 (4), 156–159.
- (36) Ashkin, A.; Dziedzic, J. M.; Bjorkholm, J. E.; Chu, S. Observation of a Single-Beam Gradient Force Optical Trap for Dielectric Particles. *Opt. Lett.* **1986**, *11* (5), 288–290.
- (37) Saija, R.; Denti, P.; Borghese, F.; Maragò, O. M.; Iatì, M. A. Optical Trapping Calculations for Metal Nanoparticles Comparison with Experimental Data for Au and Ag Spheres. *Opt. Express* **2009**, *17* (12), 10231.
- (38) Hidnert, P. Thermal Expansion of Five Selected Optical Glasses. J. Res. Natl. Bur. Stand. 1954, 52, 311-312.
- (39) Goodfriend, N. T.; Starinskiy, S. V.; Nerushev, O. A.; Bulgakova, N. M.; Bulgakov, A. V.; Campbell, E. E. B. Laser Pulse Duration Dependence of Blister Formation on Back-Radiated Ti Thin Films for BB-LIFT. *Appl. Phys. A: Mater. Sci. Process.* **2016**, *122* (3), 1–9.
- (40) Brown, M. S.; Kattamis, N. T.; Arnold, C. B. Time-Resolved Study of Polyimide Absorption Layers for Blister-Actuated Laser-Induced Forward Transfer. J. Appl. Phys. 2010, 107 (8), 083103.
- (41) Kattamis, N. T.; McDaniel, N. D.; Bernhard, S.; Arnold, C. B. Laser Direct Write Printing of Sensitive and Robust Light Emitting Organic Molecules. *Appl. Phys. Lett.* **2009**, *94* (10), 103306.
- (42) Zywietz, U.; Reinhardt, C.; Evlyukhin, A. B.; Birr, T.; Chichkov, B. N. Generation and Patterning of Si Nanoparticles by Femtosecond Laser Pulses. *Appl. Phys. A: Mater. Sci. Process.* **2014**, *114* (1), 45–50.
- (43) Kurzbach, D.; Junk, M. J. N.; Hinderberger, D. Nanoscale Inhomogeneities in Thermoresponsive Polymers. *Macromol. Rapid Commun.* **2013**, *34*, 119–134.
- (44) Duvigneau, J.; Schönherr, H.; Vancso, G. J. Nanoscale Thermal AFM of Polymers: Transient Heat Flow Effects. *ACS Nano* **2010**, *4*, 6932–6940.
- (45) Starnes, W. H. Structural Defects in Poly(Vinyl Chloride). J. Polym. Sci., Part A: Polym. Chem. 2005, 43, 2451–2467.
- (46) Jenczyk, J.; Woźniak-Budych, M.; Jarek, M.; Jurga, S. Structural and Dynamical Study of PDMS and PS Based Block Copolymers. *Eur. Polym. J.* **2018**, *98*, 384–393.
- (47) Koschwanez, J. H.; Carlson, R. H.; Meldrum, D. R. Thin PDMS Films Using Long Spin Times or Tert-Butyl Alcohol as a Solvent. *PLoS One* **2009**, *4*, No. e4572.
- (48) Liu, H.; Ascencio, J.; Perez-Alvarez, M.; Yacaman, M. Melting Behavior of Nanometer Sized Gold Isomers. *Surf. Sci.* **2001**, *491*, 88–98.

- (49) Buffat, P.; Borel, J.-P. Size Effect on the Melting Temperature of Gold Particles. *Phys. Rev. A: At., Mol., Opt. Phys.* **1976**, 13, 2287–2298
- (50) Hao, X.; Kuang, C.; Wang, T.; Liu, X. Effects of Polarization on the De-Excitation Dark Focal Spot in STED Microscopy. *J. Opt.* **2010**, 12, 115707.
- (51) Li, Q.; Ledoux-Rak, I.; Lai, N. D. Influence of Incident Beam Polariza tion on Intensity and Polarization Distributions of Tight Focusing Spot. *Adv. Device Mater.* **2015**, *1*, 4–10.